

Limits on Axion Couplings from the first 80-day data of PandaX-II Experiment

Changbo Fu,¹ Xiaopeng Zhou,^{2,*} Xun Chen,¹ Yunhua Chen,³ Xiangyi Cui,¹ Deqing Fang,⁴ Karl Giboni,¹ Franco Giuliani,¹ Ke Han,¹ Xingtao Huang,⁵ Xiangdong Ji,^{1,6,7,†} Yonglin Ju,⁸ Siao Lei,¹ Shaoli Li,¹ Huaxuan Liu,⁸ Jianglai Liu,^{1,7} Yugang Ma,⁴ Yajun Mao,² Xiangxiang Ren,¹ Andi Tan,⁹ Hongwei Wang,⁴ Jimin Wang,³ Meng Wang,⁵ Qihong Wang,⁴ Siguang Wang,² Xuming Wang,¹ Zhou Wang,⁸ Shiyong Wu,³ Mengjiao Xiao,^{9,6} Pengwei Xie,¹ Binbin Yan,⁵ Yong Yang,¹ Jianfeng Yue,³ Hongguang Zhang,¹ Tao Zhang,¹ Li Zhao,¹ and Ning Zhou¹

(PandaX-II Collaboration)

¹*INPAC and Department of Physics and Astronomy, Shanghai Jiao Tong University, Shanghai Laboratory for Particle Physics and Cosmology, Shanghai 200240, China*

²*School of Physics, Peking University, Beijing 100871, China*

³*Yalong River Hydropower Development Company, Ltd., 288 Shuanglin Road, Chengdu 610051, China*

⁴*Shanghai Institute of Applied Physics, Chinese Academy of Sciences, 201800 Shanghai, China*

⁵*School of Physics and Key Laboratory of Particle Physics and Particle Irradiation (MOE), Shandong University, Jinan 250100, China*

⁶*Center of High Energy Physics, Peking University, Beijing 100871, China*

⁷*Tsung-Dao Lee Institute, Shanghai 200240, China*

⁸*School of Mechanical Engineering, Shanghai Jiao Tong University, Shanghai 200240, China*

⁹*Department of Physics, University of Maryland, College Park, Maryland 20742, USA*

(Dated: March 12, 2022)

We report new searches for the solar axions and galactic axion-like dark matter particles, using the first low-background data from PandaX-II experiment at China Jinping Underground Laboratory, corresponding to a total exposure of about 2.7×10^4 kg-day. No solar axion or galactic axion-like dark matter particle candidate has been identified. The upper limit on the axion-electron coupling (g_{Ae}) from the solar flux is found to be about 4.35×10^{-12} in mass range from 10^{-5} to 1 keV/ c^2 with 90% confidence level, similar to the recent LUX result. We also report a new best limit from the ^{57}Fe de-excitation. On the other hand, the upper limit from the galactic axions is on the order of 10^{-13} in the mass range from 1 keV/ c^2 to 10 keV/ c^2 with 90% confidence level, slightly improved compared with the LUX.

Various theories beyond the Standard Model have predicted new weakly-coupled light $U_A(1)$ Goldstone bosons [1–5], which may answer many fundamental questions related to CP violation, possible Lorentz violation, dark matter [6–9], etc. The axion, a pseudo-scalar Goldstone boson introduced by Wilczek [10] and Weinberg [11], arises when the so-called Peccei-Quinn symmetry [1] in quantum chromodynamics (QCD) is spontaneously broken, which provides a natural solution to the so-called “strong CP problem” in QCD.

Different experimental methods [12] have been employed to search for the QCD axion or axion-like particles (ALPs), including the helioscopes [13], Light Shining through a Wall [14], microwave cavities [15], nuclear magnetic resonance [16], and the so-called axioelectrical effect [17]. Similar to the photoelectric effect, an axioelectrical effect refers to that an axion or ALP is absorbed by a bound electron in an atom, producing a free electron emission, i.e:

$$a + e + Z \rightarrow e' + Z. \quad (1)$$

The cross section for this process is related to that of the photoelectric effect through [18, 19],

$$\sigma_{Ae}(E_A) = \sigma_{pe}(E_A) \frac{g_{Ae}^2}{\beta} \frac{3E_A^2}{16\pi\alpha m_e^2} \left(1 - \frac{\beta^{2/3}}{3}\right), \quad (2)$$

where σ_{pe} is the photoelectric cross section, g_{Ae} the coupling constant between the axion and electron, E_A the incident axion energy, α the fine structure constant, m_e the mass of electron, and $\beta = v/c$ the axion velocity. The recoiling electron kinetic energy is $E_A - E_B$, where E_B is the binding energy of the electron. Therefore, the recoiling electron signals (ER) in direct dark matter search experiments can be used to search for axions or ALPs. Previous reports on the axion couplings from dark matter experiments can be found in the Ref. [19–26].

PandaX, located at China Jinping Underground Laboratory (CJPL), is a series of experiments utilizing the xenon time-projection-chamber detectors. The total mass in the target is about 120 kg in PandaX-I [29, 30], and about 580 kg in PandaX-II [31, 32]. By combining the prompt scintillation photons ($S1$) and the delayed electroluminescence photons ($S2$), PandaX has excellent (\sim cm) vertex reconstruction capabilities, which allow powerful background suppression via self-shielding and fiducialization. To set the scale, the ER background rate in PandaX-II has reached a very low level of 2.0×10^{-3} evt/keV/day ($=2.0$ mDRU), which makes it a highly sensitive detector to search for axion-electron scattering. In this paper, we report the new constraints on axion/ALP electron coupling strength g_{Ae} by using the first low-background data in PandaX-II experiment

(Run 9) with a total exposure of about 2.7×10^4 kg-day, one of the largest reported xenon data sets in the world to date.

As in Ref. [31], the Run 9 data was divided into 14 time bins according to the temporal change of detector parameters and background rates. For each event, the electron-equivalent energy E_{ee} was reconstructed from $S1$ and $S2$ as

$$E_{ee} = \frac{S1}{PDE} + \frac{S2}{EEE \times SEG}, \quad (3)$$

where PDE, EEE, and SEG are photon detection efficiency, electron extraction efficiency, and single electron gain, respectively. Most of the data cuts were identical to those in Ref. [31, 32], except we enlarged the energy window of search by replacing the upper $S1$ and $S2$ cuts with a single cut of $E_{ee} < 25$ keV. Based on the tritiated methane (CH_3T) calibration, the detection threshold was determined to be 1.29 keV, and in high energy region the detection efficiency was 94%. In total, 942 candidate events survived. The distribution of these events in $\log_{10}(S2/S1)$ vs. reconstructed energy is shown in the upper panel in Fig. 1 as the red dots. For comparison, the distribution bands corresponding to the ER calibration data from the tritium with a β -decay end point at 18.6 keV is overlaid in the figure (shadow dots). The physical data are largely consistent with ER events. The measured combined energy spectrum is shown in the lower panel of Fig. 1. In the energy range shown, the ER background is dominated by ^{85}Kr (flat) and ^{127}Xe (peak around 5 keV).

The solar axions may be produced through the following processes [19]: Compton-like scattering (C), axion-Bremsstrahlung (B), atomic-recombination (R), and atomic-deexcitation(D). Given g_{Ae} , they can all be calculated.

We took the calculations from Ref. [33] as our input axion spectrum for the axion energy range of $E_A < 10$ keV, which is valid for an axion mass less than 1 keV/ c^2 . As shown in Fig. 2, towards the lower energy (1–2 keV), the flux is dominated by axion-Bremsstrahlung process, and at the high energy region (9–10 keV), by Compton-like scattering.

Additionally, deexcitation of $^{57}\text{Fe}^*$ may also generated monoenergetic axions, i.e. $^{57}\text{Fe}^* \rightarrow ^{57}\text{Fe} + a + 14.4$ keV [34]. This monoenergetic axion flux at the Earth's orbit was estimated to be [19, 35]:

$$\Phi_{14.4} = 4.56 \times 10^{23} \cdot (g_{AN}^{\text{eff}})^2 \left(\frac{k_A}{k_\gamma} \right)^3 \text{ cm}^{-2} \text{ s}^{-1} \quad (4)$$

where k_A/k_γ is the momentum ratio between the axion and the gamma, and the g_{AN}^{eff} is a model and axion mass-dependent coupling constant between the axion and nucleus. In this work, we took the benchmark function of g_{AN}^{eff} in the so-called Dine-Fischler-Srednicki-Zhitnitskii (DFSZ) model as in Ref. [19].

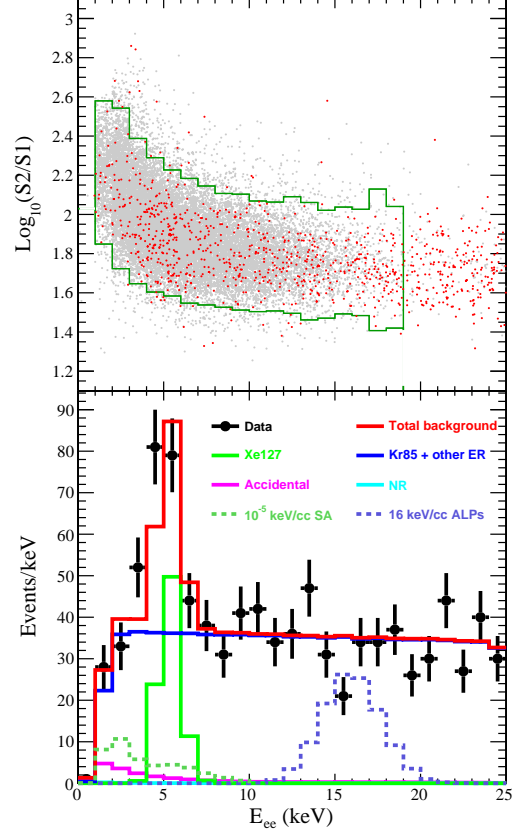


FIG. 1: Upper: Event distribution obtained in $\log_{10}(S2/S1)$ vs. E_{ee} in PandaX-II experiment; The $\pm 2\sigma$ contours for CH_3T calibration data is indicated as the green box, and the dark matter data are drawn as red crosses. Lower: the combined energy spectrum with data (histogram with uncertainties) compared to the best fit (red histogram), with individual background components indicated (see Ref. [31]). We also plot here the estimated 10^{-5} keV/ c^2 solar axion and 16 keV/ c^2 ALPs spectra assuming that g_{Ae} equals 5×10^{-12} and 5×10^{-13} respectively. See text for details.

The axion (or ALP) flux from the Milky Way dark matter (MWDM) halo can be estimated as follows. The MWDM density at the Earth location is $\rho_{\text{DM}}^{(E)} \simeq 0.3$ GeV/ cm^3 [36]. If all the MWDM is composed of ALPs, the corresponding ALP flux Φ_A can then be written as

$$\Phi_A = \rho_{\text{DM}}^{(E)} \cdot v_A / m_A = 9 \times 10^{15} \frac{\beta}{m_A}, \quad (5)$$

where v_A is the axion velocity relative to the Earth, m_A is the axion mass in unit keV/ c^2 , and $\beta = v_A/c$. Considering the same axion electron scattering mechanism, the

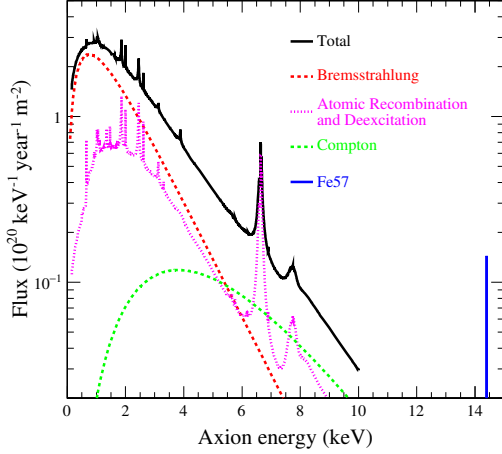


FIG. 2: The expected solar-axion flux at the earth's orbit deduced from theoretical models [19]. Five mechanisms are considered here: Compton-like scattering (C), axion-bremsstrahlung (B), atomic-recombination (R), and atomic-deexcitation (D). See the text for details. The 14.4 keV line is generated by $^{57}\text{Fe}^*$ deexcitation. In this plot, the corresponding axion parameters are set to be $g_{Ae} = 10^{-13}$ and $g_{AN}^{eff} = 10^{-8}$.

expected ALP detection rate R can be expressed as [37]:

$$R \simeq g_{Ae}^2 \left(\frac{1.2 \times 10^{19}}{A} \right) \left(\frac{m_A}{\text{keV}/c^2} \right) \left(\frac{\sigma_{pe}}{\text{barn}} \right) \text{kg}^{-1} \text{day}^{-1}, \quad (6)$$

where $A = 131.9$ is the average mass number of the xenon.

PandaX-II data can be fitted by combining the axion signal and background models. The axion or ALP signals are computed by combining incident fluxes above with the axion-electron scattering cross section in Eq. (2). The background estimates are identical to those in Ref. [31], including ^{127}Xe , ^{85}Kr and other ER background, accidental, and nuclear recoil (NR) backgrounds. As in Ref. [31], Geant4-based [38] simulation using NEST [39] ER and NR models, together with the efficiencies in $S1$ and $S2$, produce the signal and background probability distribution functions in $S1$ and $S2$. For illustration, an example axion or ALP signal is overlaid in the lower panel of Fig. 1. For each pair of values of axion mass and g_{Ae} , profile likelihood ratio statistic [40] is constructed. The likelihood function [31] used here is

$$\mathcal{L}_{\text{pandax}} = \left[\prod_{n=1}^{\text{bins}} \mathcal{L}_n \right] \times \left[\text{Gauss}(\delta_A, \sigma_A) \prod_b \text{Gauss}(\delta_b, \sigma_b) \right], \quad (7)$$

where

$$\mathcal{L}_n = \text{Poisson}(N_m^n | N_{\text{ept}}^n) \times \left[\prod_{i=1}^{N_m^n} \left(\frac{N_A^n (1 + \delta_A) P_A^n(S1^i, S2^i)}{N_{\text{ept}}^n} \right) + \sum_b \frac{N_b^n (1 + \delta_b) P_b^n(S1^i, S2^i)}{N_{\text{ept}}^n} \right]. \quad (8)$$

N_m is the event number measured experimentally, and N_{ept} is the expected event number. Axion (or ALPs) and background numbers are represented as N_A and N_b . Their probability distribution functions (PDFs), P_A and P_b , are generated using NEST-based models. Here background was divided in five independent components, ^{127}Xe , ^{85}Kr , other ER, accidental coincidence and neutron. σ and δ are systematic uncertainties and nuisance parameters for individual components with values listed in Ref. [31].

For all channels we considered, data are consistent with no axion signals. For the solar axion from the CBRD mechanisms shown above, the results are presented in Fig. 3, in which the 90% confidence level (CL) is shown as the red solid curve. The upper limit of g_{Ae} is set to about $g_{Ae} \leq 4 \times 10^{-13}$ with 90% CL in the axion mass range of $10^{-5} < m_A < 1 \text{ keV}/c^2$, similar to the recent limit from the LUX experiment [26]. Due to the high temperature in the solar core, the axion flux is generally independent of its mass, and the axioelectrical cross section picks up a gentle β -dependence (Eq. (2)) only when m_A gets closer $1 \text{ keV}/c^2$. Therefore, this limit is largely independent of the axion mass. The constraint from the ^{57}Fe 14.4 keV axion is drawn as red dotted line. The most sensitive upper limit on g_{Ae} is set at 6×10^{-14} at $m_A = 10 \text{ keV}/c^2$, which represents the best such limit to date. The fast decline of sensitivity for lower and higher mass is primarily due to the linear mass dependence of g_{AN}^{eff} in the benchmark DSFZ model [41], and the axion momentum dependence in Eq. (4), respectively.

The limits on the galactic ALPs are shown in Fig. 4. The 90% limit on g_{Ae} is set to be about $\leq 4 \times 10^{-13}$ in the mass range $1 < m_A < 25 \text{ keV}/c^2$. This limit is about 3–10 times improved from the results from XENON100, CDEX-II, and MAJORANA DEMONSTRATOR [22, 25, 27], and slightly improved from the LUX's recent result [26]. The slightly weakened limit between 4–6 keV/c^2 is due to the ^{127}Xe background in our detector, as shown in the lower panel of Fig. 1.

In summary, using the first low-background dark matter search data from PandaX-II experiment and via the axioelectrical effects, we have set new limits on the axion-electron coupling constant g_{Ae} for solar axions and galactic ALPs. For the solar axions, the limit g_{Ae} is 4.35×10^{-11} for axion mass between 10^{-5} to $1 \text{ keV}/c^2$, similar to the recent limits from LUX [26]. Best limit on g_{Ae} from ^{57}Fe axion is also reported, with the lowest exclusion

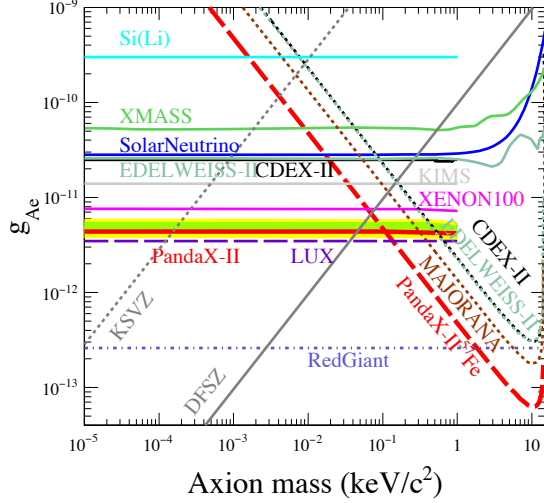


FIG. 3: The 90% upper limits on solar CBRD axion (solid red line) and 14.4 keV ^{57}Fe solar axion in g_{Ae} vs. m_A . The constraints from other representative experiments are also shown, including those using solar neutrinos [42], and data from Si(Li) target [43], CDEX-II [22], XMASS [23], EDELWEISS-II [19], KIMS [28], XENON100 [24], LUX [26], MAJORANA DEMONSTRATOR [27] (converted to g_{Ae} using the same benchmark DSFZ model values for g_{AN}^{eff} as in this paper), and observations of Red Giant [44]. The benchmarks of the QCD axion models, DFSZ [19, 41] and KSVZ (Kim-Shifman-Vainstein-Zakharov) [19, 45], are also displayed.

limit of 6×10^{-14} at a mass of 10 keV/ c^2 . For the galactic ALPs, g_{Ae} is constrained to be $< 4.3 \times 10^{-14}$ (90% C.L.) for an axion mass between 1 to 25 keV/ c^2 , which represents the strongest constraints to date. PandaX-II will continue taking data, and more sensitive search of axion is expected in the future.

This project has been supported by a 985-III grant from Shanghai Jiao Tong University, grants from National Science Foundation of China (Nos. 11365022, 11435008, 11455001, 11505112 and 11525522), and a grant from the Ministry of Science and Technology of China (No. 2016YFA0400301). We thank the support of grants from the Office of Science and Technology, Shanghai Municipal Government (No. 11DZ2260700, No. 16DZ2260200), and the support from the Key Laboratory for Particle Physics, Astrophysics and Cosmology, Ministry of Education. This work is supported in part by the Chinese Academy of Sciences Center for Excellence in Particle Physics (CCEPP) and Hongwen Foundation in Hong Kong. Finally, we thank the following organizations for indispensable logistics and other supports: the CJPL administration and the Yalong River Hydropower Development Company Ltd.

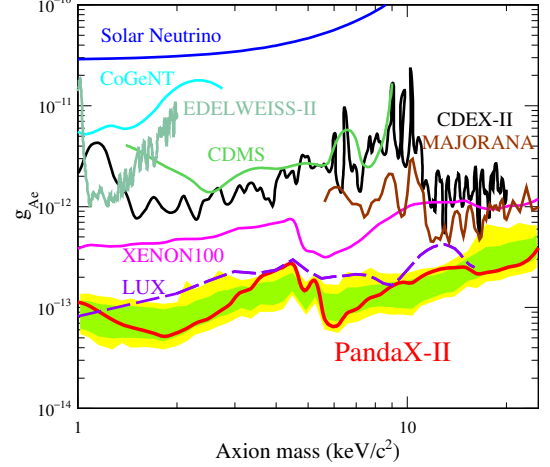


FIG. 4: Constraints on g_{Ae} as a function of MWDM ALP mass. PandaX's 90% limit is shown as the red curve, with $\pm 1\sigma$ and $\pm 2\sigma$ sensitivity bands in green and yellow respectively. The constraints from other representative experiments are also shown, including those from the solar neutrinos [42], data from CDEX-II [22], CoGeNT [21], CDMS [20], EDELWEISS-II [19], XENON100 [25], LUX [26] and MAJORANA DEMONSTRATOR [27].

* Corresponding author:zhouxp@pku.edu.cn

† PandaX Spokesperson, xdji@sjtu.edu.cn

- [1] R. D. Peccei and H. R. Quinn, Phys. Rev. Lett. **38**, 1440 (1977).
- [2] C. T. Hill and G. G. Ross, Nucl. Phys. B **311**, 253 (1988).
- [3] E. Gildener and S. Weinberg, Phys. Rev. D **13**, 3333 (1976).
- [4] D. J. E. Marsh, Phys. Rep. **643**, 1 (2016).
- [5] J. Jaeckel and A. Ringwald, Ann. Rev. Nucl. & Part. Sci. **60**, 405 (2010).
- [6] J. Leitner and S. Okubo, Phys. Rev. **136**, B1542 (1964).
- [7] J. E. Kim and G. Carosi, Rev. Mod. Phys. **82**, 557 (2010).
- [8] C.-G. Shao, Y.-J. Tan, et al., Phys. Rev. Lett. **117**, 071102 (2016).
- [9] L. Covi, H. Kim, J. Kim, and L. Roszkowski, J High Eng. Phys. p. 033 (2001).
- [10] F. Wilczek, Phys. Rev. Lett. **40**, 279 (1978).
- [11] S. Weinberg, Phys. Rev. Lett. **40**, 223 (1978).
- [12] P.W. Graham, I.G. Irastorza, S.K. Lamoreaux, A. Lindner, K.A. van Bibber, Annu. Rev. Nucl. Part. Sci. **65**, 485 (2015).
- [13] K. Zioutas, M. Tsagri, Y. Semertzidis, et al., New Journal of Physics **11**, 105020 (2009).
- [14] E. Klaus, F. Maik, G. Samvel, et al., Phys. Lett. B **689**, 149 (2010).
- [15] R. Bradley, J. Clarke, D. Kinion, et al., Rev. Mod. Phys. **75**, 777 (2003).

- [16] H. Yan, G. Sun, S. Peng, et al., Phys. Rev. Lett. **115**, 182001 (2015).
- [17] F. T. Avignone III, R. L. Brodzinski, S. Dimopoulos, et al., Phys. Rev. D **35**, 2752 (1987).
- [18] A. Derevianko, V. A. Dzuba, V. V. Flambaum, and M. Pospelov, Phys. Rev. D **82**, 065006 (2010).
- [19] E. Armengaud, Q. Arnaud, C. Augier, et al., J. Cosmol. Astropart. Phys. **2013**, 067 (2013).
- [20] Z. Ahmed, D. S. Akerib, et al. (CDMS Collaboration), Phys. Rev. Lett. **103**, 141802 (2009).
- [21] C. E. Aalseth, P. S. Barbeau, et al. (CoGeNT Collaboration), Phys. Rev. Lett. **106**, 131301 (2011).
- [22] S. K. Liu, Q. Yue, et al. (CDEX Collaboration), Phys. Rev. D **95**, 052006 (2017).
- [23] K. Abe, K. Hieda, et al. (XMASS Collaboration), Physics Letters B **724**, 46 (2013).
- [24] E. Aprile, F. Agostini, et al. (XENON100 Collaboration), Phys. Rev. D **90**, 062009 (2014).
- [25] E. Aprile, F. Agostini, et al. (XENON100 Collaboration), Phys. Rev. D **95**, 029904 (2017).
- [26] D. S. Akerib, S. Alsum, et al. (LUX Collaboration) (2017), Phys. Rev. Lett. **118**, 261301 (2017).
- [27] N. Abgrall, I.J. Arnquist, et al. (Majorana Collaboration) (2017), Phys. Rev. Lett. **118**, 161801 (2017).
- [28] Y.S. Yoon, H.K. Park, et al. (KIMS Collaboration) (2016), JHEP **06**, 011 (2016).
- [29] M. Xiao, X. Xiao, L. Zhao, et al., Sci. China Phy. Mech. & Astro. **57**, 2024 (2014).
- [30] X. Xiao, X. Chen, A. Tan, et al. (PandaX Collaboration), Phys. Rev. D **92**, 052004 (2015).
- [31] A. Tan, M. Xiao, X. Cui, et al. (PandaX-II Collaboration), Phys. Rev. Lett. **117**, 121303 (2016).
- [32] C. Fu, X. Cui, X. Zhou, et al. (PandaX-II Collaboration), Phys. Rev. Lett. **118**, 071301 (2017).
- [33] J. Redondo, J. Cosmol. Astropart. Phys. **2013**, 008 (2013).
- [34] S. Moriyama, Phys. Rev. Lett. **75**, 3222 (1995).
- [35] S. Andriamonje, S. Aune, et al. (CAST collaboration), J. Cosmol. Astropart. Phys. **2009**, 002 (2009).
- [36] A. M. Green, Modern Physics Letters A **27**, 1230004 (2012).
- [37] M. Pospelov, A. Ritz, and M. Voloshin, Phys. Rev. D **78**, 115012 (2008).
- [38] S. Agostinelli, J. Allison, et al., Nucl. Instrum. Methods Phys. Res. A **506**, 250 (2003), ISSN 0168-9002.
- [39] B. Lenardo, K. Kazkaz, A. Manalaysay, J. Mock, M. Szydagis, and M. Tripathi, IEEE Trans. Nucl. Sci. **62**, 3387 (2015), 1412.4417.
- [40] E. Aprile, K. Arisaka, et al. (XENON100 Collaboration), Phys. Rev. D **84**, 052003 (2011).
- [41] M. Dine, W. Fischler, and M. Srednicki, Phys. Lett. B **104**, 199 (1981).
- [42] P. Gondolo and G. G. Raffelt, Phys. Rev. D **79**, 107301 (2009).
- [43] A. V. Derbin, JETP Lett. **95**, 379 (2012).
- [44] N. Viaux, M. Catelan, P. B. Stetson, G. G. Raffelt, J. Redondo, A. A. R. Valcarce, and A. Weiss, Phys. Rev. Lett. **111**, 231301 (2013).
- [45] M. A. Shifman, A. Vainshtein, and V. I. Zakharov, Nucl. Phys. B **166**, 493 (1980).